# Monitoring the high-altitude cusp with low-energy neutral atom imager: Simultaneous observations from IMAGE and Polar

S. Taguchi,[1] S.-H. Chen,[2] M. R. Collier,[3] T. E. Moore,[3] M.-C. Fok,[3] K. Hosokawa,[1] and A. Nakao[1]

[1]Department of Information and Communication Engineering, University of Electro-Communications, Chofu, Tokyo, 182-8585, Japan

[2]Universities Space Research Association, NASA Goddard Space Flight Center, Greenbelt, MD 20771

[3] NASA Goddard Space Flight Center, Greenbelt, MD 20771

Correspondence to: taguchi@ice.uec.ac.jp

Running title: Cusp observations from IMAGE and Polar

Submitted to Journal of Geophysical Research (Revised version)

August 2005

**Abstract**. The Low Energy Neutral Atom (LENA) imager on the IMAGE spacecraft in the dayside magnetosphere can detect neutral particles that are emitted in the magnetosheath flow. During a period of dynamic pressure of 4-6 nPa and IMF $B_Z$ of –5 to 3 nT on April 12, 2001, LENA on IMAGE at ($X_{GSM}$, $Y_{GSM}$, $Z_{GSM}$)~(4 $R_E$, 0 $R_E$, 6 $R_E$) observed significant emission in the direction of the high-latitude magnetosheath. Detailed analyses have revealed that the high-latitude sheath emission consists of two parts: the stable emission at the higher-latitudes, and the lower-latitude emission that occurs on and off. During the interval of this event, the Polar spacecraft was located at somewhat lower latitudes than IMAGE in similar noon meridian, and the plasma observations with the Thermal Ions Dynamic Experiment showed that the entry of the cusp ions happens in concurrence with the appearance of the lower-latitude LENA emission. This coincidence strongly suggests that the cusp ions flowing earthward charge-exchange with the hydrogen exosphere. For the higher-latitude emission, its stability suggests that the source is associated with the structure persistently existing, which is consistent with the recent result showing that the sheath flow in the cusp indentation can create neutral atom emissions. Comparison between the LENA emission and ACE solar wind suggests that the lower-latitude LENA emission occurs during the southward tilting of dawnward IMF, indicating that this emission is associated with the earthward ion flux along the newly reconnected field lines. Hence, this unique event for the simultaneous observations strongly suggests that LENA monitors the entry of the ions in the cusp, which is triggered by the southward tilting of IMF, and that the significant flux of the cusp ion entry occurs equatorward of, and separately from the cusp indentation.

**1. Introduction.**

In understanding mass and energy deposition in the magnetosphere and ionosphere from the solar wind, the position and motion of the polar cusp is of great importance. The effect of the solar wind on the polar cusp has been extensively examined at low altitudes using plasma observations from spacecraft [e.g., Burch et al., 1973; Meng, 1983; Newell and Meng, 1988], and from observations of auroral emission using optical ground-based techniques [e.g., Sandholt et al., 1994, 1998]. Recent studies with the satellite-borne aurora imager have added new features to our understanding of the cusp for the northward interplanetary magnetic field (IMF) [Milan et al., 2000; Fuselier et al., 2002]. The characteristics of the low-altitude cusp are now well understood, including its temporal variations with a time resolution of several minutes.

The effect of the solar wind on the polar cusp at altitudes of about 5 to 9 $R_E$ has been examined in detail with the Polar spacecraft. Zhou et al. [2000] identified a significant number of polar cusp crossings, and clarified the characteristics of the position of the polar cusp, including its dependence on the solar wind. At these altitudes, the cusp region is larger than at the top of the ionosphere because of the magnetic-field geometry. In addition, since the spacecraft moves more slowly here than in a low-altitude orbit, a typical cusp crossing at the altitude of Polar takes about 30 min [e.g., Zhou et al., 2000], which is much longer than the crossing time at ionospheric height (1–2 minute).

At higher altitudes than Polar, the cusp observations have an even longer period. Hawkeye spacecraft, which can traverse at altitudes greater than 10 $R_E$, has revealed well-defined cusp crossings [e.g., Farrell and Van Allen 1990]. The typical duration of these cusp crossings appears to be about 1 hour.

It would seem that such long-duration cusp observations (~30 min to 1 hour), may exceed the several-minute response time of the cusp to solar wind variations. In other words, results from analyses of the well-defined interval of the cusp crossing at such high altitudes reflect the cusp response to the solar wind for a timescale longer than ~30 min. To deduce the shorter timescale response, the field and plasma variations embedded in the large-scale structure must be examined as far as *in-situ* spacecraft observations are concerned.

Using Hawkeye data, Chen et al. [1997] presented an event identified in a possible location of the cusp indentation, and related the observed plasma and magnetic field variations, which had a timescale of several minutes, with the motion of the cusp as modulated by the varying IMF. Collection of this kind of event from *in situ* observations is expected to advance our understanding of the cusp dynamics at high altitudes. However, in using a single spacecraft it is difficult to find many cusp-crossing events that can be correlated with solar wind variations with a timescale of several minutes, because plasma and magnetic field data obtained in the cusp often include irregular or turbulent variations [Dunlop et al., 2000].

Recent remote sensing studies with the low energy neutral atom (LENA) imager [Moore et al., 2000] on the IMAGE spacecraft have shed new light on the understanding of the dynamics of the high-altitude cusp. Extending the finding that neutral particles detected by LENA in the magnetosphere include the result of solar-wind ions charge-exchanging with the hydrogen exosphere in the magnetosheath flow [Collier et al., 2001ab, Fok et al., 2003, Moore et al., 2003], Taguchi et al. [2004] have shown that the LENA emissions observed in the direction of the high-latitude magnetosheath during high dynamic pressures of ~20 nPa reflect the cusp indentation in the magnetopause shape, which suggests a means for monitoring the cusp motion using LENA.

In this paper, we examine an IMAGE/LENA emission event for a period of moderately high dynamic pressure of 4-6 nPa on April 12, 2001. Results of analyses show that the LENA emission in the direction of the high-latitude sheath consists of two parts: the stable emission at the higher-latitudes, and the lower-latitude emission that occurs on and off. We also show that appearance of the latter lower-latitude emission is consistent with the observation with the Thermal Ions Dynamic Experiment (TIDE) and the magnetic field experiment (MFE) on the Polar spacecraft located somewhat at lower latitudes than IMAGE in the similar noon meridian. This consistency indicates that the entry of the cusp ions creates the LENA emissions, and that monitoring this entry with LENA is possible. Coupled with the existence of the emission at higher latitudes, which has been recently interpreted as the signal from the cusp indentation, we suggest that the significant flux of the cusp ion entry occurs equatorward of, and separately from the cusp indentation.

## 2. Solar Wind Conditions

Figure 1 shows the solar wind conditions for the event that we analyzed in this study together with the SYM-H index. The ACE spacecraft was located about 200 $R_E$ upstream of the Earth. To check if energetic ions with energies of $\geq$50 keV/e (which is well above nominal upper limit on energy for LENA response) do not cause unexpected variation by penetrating the LENA collimator, we first examined solar wind ions with energies between 47 and 65 keV/e from the ACE Electron, Proton, and Alpha Monitor. The energetic ion data are plotted in Panel a. The variation is very gradual, which suggests that if the energetic ions penetrating the collimator cause LENA variation, it would be a relatively constant effect. In other words, if the LENA response varies with timescales much shorter than the very gradual variations of the solar wind energetic ions, it strongly suggests that the LENA response is not due to the energetic ions [Collier et al., 2001a]. As is shown later, LENA observed emissions that occurs on and off with timescales of several minutes.

Panels b and c of Figure 1 show respectively the IMF $B_Y$ and $B_Z$ in GSM coordinates. We plotted 64-s averages of IMF data that were created from original 16-s averages so as to make comparison between the IMF and plasma data easier. During the plotted interval $B_Y$ is negative, and the dominant component. $B_Z$ varies mostly between ±3 nT in the first half of the interval, and becomes persistently negative after that. The $B_X$ component varies mostly between ±5 nT through the interval (not shown).

The solar wind dynamic pressure in Panel f of Figure 1 was calculated from the density (panel d) and speed (panel e) assuming 4% $He^{++}$ particles. Panel g shows the H-component of the SYM index [Iyemori and Rao, 1996]. We related the start of a sharp increase of the solar wind dynamic pressure at 0355 UT (left line in Panels d, e, and f) and a decrease at 0443 UT (right line) with a positive sudden impulse ($SI^+$) at 0422 UT and a negative sudden impulse ($SI^-$) [Araki and Nagano, 1988; Takeuchi et al., 2002] at 0514 UT, respectively. The time lag from ACE to Earth is then estimated to be 27-31 min.

## 3. Emission observed by IMAGE/LENA

Figure 2 illustrates where is the suitable position for monitoring the cusp indentation. When the sheath ion flow comes to the cusp indentation, neutral hydrogen can be emitted if there is adequate charge-exchanging of ions with the hydrogen exosphere which is illustrated with several concentric circles. These circles simply represent that the exospheric neutral hydrogen densities are spherically symmetric [Wallace et al., 1970; Rairden et al., 1986], and their color does not reflect any density profiles. Note, however, that a slight asymmetry exists in the actual density profiles [Ostgaard et al., 2003].

For simplicity, only three representative directions of the possible emission are shown (green arrows). When the spacecraft is situated as is shown in Figure 2, the spacecraft would observe clearly neutral hydrogen emitted in the direction of the arrow shown as Emission A. A simple model by Taguchi et al. [2004] has shown that this kind of emission can be observed as a distinct peak in the distribution of the hydrogen count (their Figure 5).

For remote sensing of the cusp indentation, it is important that the emission does not overlap with neutral atoms coming directly from the Sun, because this flux, which is called the Sun signal [e.g., Moore et al., 2001; Collier et al., 2001a, 2003], is stronger than the emission in the direction of the cusp indentation. Emission B can be parallel to the Sun–Earth line, and would overlap the Sun signal when the spacecraft is located downstream of Emission B. Emission C can also overlap stronger emission when the spacecraft is located downstream of Emission C. The stronger emission may come from the magnetosheath near the equatorial plane [Collier et al., 2005; Taguchi et al., 2004]. Hence, a spacecraft residing at a somewhat smaller $Z$ than the possible location of the indentation would be suitable for monitoring the cusp.

The sheath flow may slow down when it intrudes into the cusp indentation. This possible slowdown is favorable for LENA's cusp monitoring because there is a high probability that the flow in the cusp will stay within the nominal energy upper limit for the response of LENA to ions (converted negative ions) that the incident neutrals become by picking up an electron from the conversion surface inside LENA.

Neutral atoms from the sheath would include components having higher energies than the nominal energy upper limit for the response of LENA. Since such energetic neutral atoms can cause “sputtering” of negative ions from the conversion-surface of LENA, the negative ions, which have much lower energies than the incident neutrals, can be detected inside LENA [Collier et al., 2001a]. For this reason, LENA can respond to incident neutrals with energies of up to at least 3-4 keV [Moore et al., 2003], and cover the high-energy component of the sheath ions. This capability would make the angular dispersion of the sputtered ions broader than the incident signal. Hence, we did not examine the detail of spatial broadening of the incident signals, but analyzed the signals by focusing on the location of the peak count in a LENA snapshot.

Figures 3a and 3b show the IMAGE orbit in the $X_{GSM}$-$Z_{GSM}$ and $X_{GSM}$-$Y_{GSM}$ planes for the interval that we analyzed in this paper, respectively. IMAGE is located near ($X_{GSM}$, $Z_{GSM}$)~(4 $R_E$, 6 $R_E$) in the mid-noon sector ($Y_{GSM}$= −0.5 $R_E$). Polar is located at somewhat lower latitudes than IMAGE, and in similar noon meridian plane.

In Figure 3a, two arrows from the starting location on the IMAGE orbit indicate the approximate projection of a 120˚ field of view of LENA to the $Y_{GSM}$=0 meridian. The upward arrow indicates the upper boundary of the 120˚, which was decided as an 8˚-bin whose LOS makes the minimum angle from the $Z$-axis [Taguchi et al., 2004]. The other arrow represents the lower boundary, which corresponds to the 8˚-bin that covers from 97˚ to 105˚. This bin is three sectors (=24˚) from the solar direction.

Figure 4 shows an example of the LENA snapshots obtained during the orbit shown in Figure 3. The background-corrected scaled hydrogen count rates observed at 0508 UT (which covers 0507 to 0509 UT) are plotted in the format of spin angle versus polar angle. The Sun signal is seen at lower spin angles. The details of the cause of the Sun signal have been reported by Collier et al. [2003, 2001a and b]. Weak emission can be seen at the spin angles much larger than those of the Sun signal. This signal has been interpreted as being created in the cusp indentation [Taguchi et al., 2004], and is referred to as the cusp indentation signal.

Three images of Figure 5 show the same image as the one in Figure 4 plus two snapshots obtained 2 min before and after. The format of each plot of Figure 5 is the GSM *Z* versus *Y*, and the values of *Y* along the horizontal axis decrease from left to right, that is, from the post-noon to the pre-noon side. The hydrogen count rate for each LOS is plotted at the ($Y_{\mathrm{GSM}}$, $Z_{\mathrm{GSM}}$) position of the intersection of a sphere surface with a radius of 8 $R_{\mathrm{E}}$

The outer boundary shown with the white rectangle of Figure 4 is drawn in Figure 5 as a distorted boundary. The region inside the distorted white boundary in Figure 5 is somewhat narrow near $Z_{\mathrm{GSM}}$ ~6.5 $R_{\mathrm{E}}$ compared with the upper and lower parts. This simply reflects that the mapping surface for the field of view in the middle part is somewhat close to the location of the spacecraft. Note that the narrowest part in the middle is not any indication of the cusp indentation structure.

In all snapshots of Figures 5 the Sun signal appears at $Z = 5\ R_{\mathrm{E}}$ to 6 $R_{\mathrm{E}}$. That emission should be seen in the *Z* position that is similar to the one for the spacecraft (Figures 3a) because it should come roughly along the *X* axis. At $Z = 6.5\ R_{\mathrm{E}}$ to 7 $R_{\mathrm{E}}$ in each plot there is another stable emission, i.e., the cusp indentation signal. The peak of this emission is indicated with the white cross mark. For Figure 5b, the position of this peak on the sphere is ($X_{\mathrm{GSM}}$, $Y_{\mathrm{GSM}}$, $Z_{\mathrm{GSM}}$) =(4.2 $R_{\mathrm{E}}$, –0.5 $R_{\mathrm{E}}$, 6.8 $R_{\mathrm{E}}$).

The field mapping based on the Tsyganenko 96 model shows that the northern ionospheric footprint is at a latitude of ~72.5˚ in corrected geomagnetic latitudes. This latitude is not inconsistent with the interpretation that the emission is the cusp indentation signal, although the input values of the IMF $B_Y$ (–15 nT) and Dst (–164 nT) for the Tsyganenko 96 model are beyond the range of reliable approximation. We note, however, that the latitude of ~72.5˚ is lower than the average of the cusp latitude for small IMF $|B_Z|$ conditions [Newell et al., 1989; Taguchi et al., 1993].

When Figure 5c is compared with Figures 5a and 5b, it is clear that emissions appear around $Z$=6.4 $R_E$ (indicated with the red cross mark), i.e., equatorward of the cusp indentation signal. We will show in the next section that this emission is in concurrence with the entry of the cusp ions at Polar.

## 4. IMAGE/LENA and Polar/TIDE Observations

The IMAGE/LENA and Polar observations for 0500-0520 UT, which include the above timing of the appearance of the LENA emission around $Z$ =6.4 $R_E$ (Figure 5c), are shown in Figure 6. The top four panels show data from the Polar magnetic field experiment (MFE) [Russell et al., 1995]. Panels e and f represent the TIDE spectrogram in spin-angle vs. UT and the one in energy vs. UT, respectively. In Panel e, the – (+) sign indicates the direction (opposite direction) of the magnetic field projected on the spin plane with respect to the spacecraft moving direction indicated by × sign (which is immediately below the – sign). If TIDE measures fluxes in the + direction which is oriented in the opposite direction of the magnetic field, it means that the entry of the ions occurs in parallel with the magnetic field.

TIDE can observe cold ions in the energy range 0.3 to 450 eV above the spacecraft potential during the 6-s spin period of the satellite [Moore et al., 1995]. We used STOPS component in TIDE data, which gives collapsed three dimensional measurements as 2D velocity distributions in the spin plane, because the STARTS component, which provides 3D measurements, was not functioning after late 1996 [Chen and Moore, 2004].

Panel g shows a LENA spectrogram for spin angles of 145˚-217˚. This range does not include the Sun signal. Counts are normalized so that the maximum peak of the hydrogen background corrected scaled count rate can be unity in each time and spin angle range [Taguchi et al., 2004]. At 0509 UT the maximum count (red region) shifted to smaller angles, i.e., to the third bin from the bottom, while keeping a minor peak (blue color) at higher angles. In other words, the distribution becomes a double peak structure (Figure 5c).

This timing is concurrent with the Polar/TIDE observations of the significant ion flux, which are shown in Panels e and f. Before ~0509:30 UT the energy flux at Polar is relatively low, indicating the tenuous magnetospheric population. After that, the higher energy-flux is observed in concurrence with the depression of the total magnetic field (Panel d), that is, the entry of the cusp ions is identified. The left vertical line (at 0510 UT) indicates the time when the depression of the magnetic field starts. The maximum depression occurs around 0511 UT, and the decrease of $|B|$ from 0510 to 0511 UT is about 20 nT. Around 0512:10 UT the magnetic field returns the background level. This time is shown with the right vertical line.

The ion distribution at a period between the two lines (Panel e) has a field-aligned flow, i.e., the entry of the ions along the magnetic field as far as it is observed with a low energy instrument, TIDE. From the concurrence of the cusp ion entry at Polar/TIDE with the appearance of the LENA emission at the smaller angle bins at 0509-0513 UT (Panel g), it is strongly suggested that the cusp ion entry creates the neutral atom emission through charge exchanging with hydrogen exosphere.

After that, Polar entered the magnetospheric population (0513-0515 UT). Then it again observed relatively high energy-flux in concurrence with the small depression of the total magnetic field at 0515-0516 and 0517-0518 UT. From these multiple occurrences of the cusp-like properties, it seems that the cusp observation around 0510 UT is not the traversal of the stationary whole cusp structure. Rather, it would be related to some temporal change, for example, the motion of the region of the ion entry. We note that the encounter of the cusp ion entry in the present observation is short when compared with the typical cusp crossing at the altitude of Polar, i.e., about 30 min [e.g., Zhou et al., 2000].

We show simple categorization of the LENA and TIDE observations below Panel g. In this categorization S or D before the slash means that the LENA emission is single or double, respectively. The letter after the slash, C or NC represents whether Polar observed the cusp ion entry or the non-cusp, respectively.

As mentioned above, Polar appears to be in the cusp-like population after 0515 UT. However, since the energy flux is somewhat lower and the magnetic depression is smaller during such a period of time than during 0510-0512 UT when the typical cusp ion entry occurs, it is hard to tell unambiguously whether the region is a part of the cusp or not. We have just shown this situation as "D/C or D/NC." During such an interval the LENA emission has a double structure. The LENA double emission can be also seen at 0503-0505 UT. During this interval, Polar was in the magnetospheric population, i.e., the non-cusp.

Panel h shows 31-min delayed ACE $B_Z$ data. This time delay comes from the estimation made in Figure 1. It is clear that the appearance of the LENA lower-latitude emission at 0509 UT is in concurrence with the negative change of the IMF $B_Z$, and that the double emission continues during the interval of the negative IMF $B_Z$. The agreement between the double emission and the negative $B_Z$ can be also seen around 0504 UT. Hence, the appearance of the lower-latitude emission, which is concurrent with the significant flux of the cusp ions at Polar, is associated with the southward tilting of IMF.

## 5. Discussion and Conclusions

When IMF $B_Z$ is negative, reconnection occurs on the dayside magnetopause. Newly reconnected flux tubes pass through the cusp entry layer, where the ions move earthward along the magnetic field lines. These ions would produce neutral atoms when they reach the place where the hydrogen density in the exosphere is adequate. This situation is schematically shown in Figure 7.

The shaded region in Figure 7 represents the region where the entry of ions occurs, i.e., the plasma entry layer [Paschmann et al., 1976] or the interior cusp [Chen et al., 1997]. The arrow from this shaded region shows the ion entry along the magnetic field line (gray line). This line represents an open field line after the reconnection.

Green dashed lines from the magnetic filed line (gray color) represent neutral atom emissions. Some of these emissions can reach the position of IMAGE, and this type of emission is identified as the lower-latitude part of the emissions. The higher-latitude part of the emissions is shown with the dashed green lines from the cusp indentation. This kind of emissions is caused by the sheath ion flow, i.e., Emission A in Figure 2. Hence, our interpretation suggests that the cusp ion entry is operative equatorward of, and separately from the cusp indentation.

We examine below if it is possible for the cusp ion entry to produce observable counts of the neutral atom emissions. From the TIDE plasma moments for 0-400 eV, the number density and velocity around 0512 UT are calculated to be 12 $cm^{-3}$ and 38 km $s^{-1}$, respectively (not shown). The number flux for this energy range is $4.6\times10^{7}$ cm$^{-2}$ s$^{-1}$. For the cusp ions, there should be a hotter component above 400 eV. To obtain the total flux, we need to include this contribution, and multiply the flux by a factor of 1~2. For example, when we take 1.5 for the factor, the ion total flux is ~$7\times10^{7}$ cm$^{-2}$ s$^{-1}$.

For simplicity, we regard the charge-exchange of the ions as being operative between the altitude of IMAGE (at $R$~7$R_E$) and $R$=10 $R_E$. The latter value reflects the distance of the model magnetopause [Shue et al., 1998] in the direction of the LENA peak emission for the corresponding solar wind conditions, i.e, $B_Z$ =0 nT, and $P_{dyn}$=5 nPa. When the LENA's field-of-view for a single spin sector falls in the region of the source ion flux, the neutral atom flux, $\Phi_N$ obtained at that spin angle is expressed as the integral of the ion flux $\Phi_{ION}$, multiplied by the charge exchange cross section σ and the hydrogen exospheric density, $n_H$ along the line of sight [Collier et al., 2001b; Taguchi et al., 2004, and reference therein]. When we assume that the line of sight is along the radial direction from the center of the Earth, and that σ and $\Phi_{ION}$ (=$7\times10^{7}$ cm$^{-2}$ s$^{-1}$) does not vary along the line of sight from $R$=7$R_E$ to $R$=10 $R_E$, $\Phi_N$ can be estimated as

$$\Phi_N = \Phi_{ION}\sigma\int_{7R_E}^{10R_E} n_H \, dR \, . \qquad (1)$$

Using the recent result for the neutral hydrogen density by Ostgaard et al. [2003] (their Figure 10), we can calculate the above integral from $R$=7 $R_E$ to $R$=10 $R_E$ to be ~$5\times10^{10}$ cm$^{-2}$. Taking σ ~$2\times10^{-15}$ cm$^{2}$ [Gealy and Van Zyl, 1987; Collier et al., 2005], we get $\Phi_N$~$7\times10^{3}$ cm$^{-2}$ s$^{-1}$. When we take $1.9\times10^{-4}$ for LENA's neutral hydrogen detection efficiency for the time period of the present observation, $\Phi_N$ of $7\times10^{3}$ cm$^{-2}$ s$^{-1}$ would correspond to a count rate of 1.3s$^{-1}$ at LENA whose entrance aperture has an area of 1 cm$^{2}$. Since each spin sector is observed for about 2.7 seconds, this count rate would be about 4 count per spin. It thus appears that the cusp ion entry produces neutral atom emissions that can be detected by LENA, although this count is somewhat lower than the actual observation, 12 count/spin in the sector for the peak of the lower-latitude emission (Figure 5c).

In Figure 6 we have shown that the lower-latitude emission continues after 0509 UT. This suggests that the ion entry occurs continuously. On the other hand, the Polar observations show that the ion entry disappears for a while after 0513 UT. From these facts, we know that the disappearance of the ion entry at Polar is due to the exit of Polar from the region of the cusp ion entry, not due to the stop of the ion entry. The reason for this interpretation is that the LENA lower-latitude peak (purple color) at 0513-0515 UT occurs at one bin larger angle than before, that is, the source moves poleward. For the double emission at 0503-0505 UT (Figure 6), there are no corresponding signatures at Polar. This indicates that Polar was still located well equatorward of the cusp entry region at that time.

In conclusion, the simultaneous observations from IMAGE/LENA and Polar/TIDE have shown that the LENA emission in the direction of the high-latitude magnetosheath consists of two parts, and that the lower-latitude emission can occur in concurrence with the entry of the cusp ions at Polar located at somewhat lower latitudes than IMAGE in similar noon meridian. This concurrence can be interpreted as the charge-exchange of the earthward flowing cusp ions with the hydrogen exosphere. This kind of neutral atom emission seems to happen during the southward tilting of IMF, suggesting that the cusp ions for this emission occur on the newly reconnected field lines. The higher-latitude emission is stable, and operative separately from the lower-latitude emission. Its stability suggests that the source is associated with the structure persistently existing, which is consistent with the recent result showing that the sheath flow in the cusp indentation can create neutral atom emissions. These observations suggest that LENA can monitor the entry of the cusp ions, and that the significant flux of the ion entry occurs equatorward of, and separately from the cusp indentation.

## Acknowledgments

The initial part of this study was made while S. Taguchi was in Universities Space Research Association, NASA/GSFC during his Sabbatical from University of Electro-Communications, Japan. S.-H. Chen's work was supported by the Polar Mission under UPN 370-08-43. This research was supported by the IMAGE Project under UPN 370-28-20 at Goddard Space Flight Center, and by grant-in-aid 15540427 in Category C under Japan Society for the Promotion of Science. A special thanks goes to Atsushi Yamazaki for his help in the interpretation. Polar magnetic field data, and ACE solar wind data are provided by NASA/NSSDC. The authors thank C. T. Russell (PI of Polar magnetic field data), D. McComas (PI of ACE plasma data), N. Ness (PI of ACE magnetic field data), and R. Gold (PI of ACE EPAM data). We also thank WDC for Geomagnetism, Kyoto, Japan for providing the midlatitude SYM-H index.

## References

Araki, T., and H. Nagano, Geomagnetic response to sudden expansions of the magnetosphere, J. Geophys. Res., 93, 3983-3988, 1988.

Burch, J. L., Rate of erosion of the dayside magnetic flux based on a quantitative study of the dependence of Polar cusp latitude on the interplanetary magnetic field, Radio Sci., 8, 955, 1973.

Chen, S.-H., S. A. Boardsen, S. F. Fung, J. L. Green, R. L. Kessel, L. C. Tan, T. E. Eastman, and J. D. Craven, Exterior and interior Polar cusps: Observations from Hawkeye, J. Geophys. Res., 102, 11,335-11,347, 1997.

Chen, S.-H., and T. E. Moore, Dayside flow bursts in the Earth's outer magnetosphere J. Geophys. Res., 109, No. A3, A03215, 10.1029/2003JA010007, 2004.

Collier, M. R., et al., Observations of neutral atoms from the solar wind, J. Geophys. Res., 106, 24,893-24906, 2001a.

Collier, M. R., et al. LENA Observations on March 31, 2001: Magnetosheath Remote Sensing, *Eos. Trans. AGU*, 82(47), Fall Meeting Suppl., Abstract SM41C-05, F1071-F1072, 2001b.

Collier, M. R., et al., Dust in the wind: The dust geometric cross section at 1 AU based on neutral solar wind observations, in Solar Wind 10, *Proceedings of the Tenth International Solar Wind Conference*, M. Velli, R. Bruno and F. Malara (eds.), AIP Conference Proceedings Volume 679, American Institute of Physics, Melville, New York, pp. 790-793, 2003.

Collier, M. R., T. E. Moore, M.-C. Fok, B. Pilkerton, and S. Boardsen, Low-energy neutral atom signatures of magnetopause motion in response to southward $B_z$, J. Geophys. Res., 110, A02102, doi:1029/2004JA010626, 2005.

Dunlop, M. W., P. J. Cargill, T. J. Stubbs, and P. Woolliams, The high-altitude cusps: HEOS 2, J. Geophys. Res., 105, 27,509-27,517, 2000.

Farrell, W. M., and J. A. Van Allen, Observations of the Earth's Polar cleft at large radial distances with the Hawkeye 1 magnetometer, J. Geophys. Res., 95, 20945-20958, 1990.

Fok, M.-C., et al., Global ENA IMAGE simulations, Space Sci. Rev., 109, 77-103, 2003.

Fuselier, S. A., H. U. Frey, K. J. Trattner, S. B. Mende, and J. L. Burch, Cusp aurora dependence on interplanetary magnetic field $B_Z$, J. Geophys. Res., 107(A7), 10.1029/2001JA900165, 2002.

Gealy, M. W., and B. Van Zyl, Cross sections for electron capture and loss. I. $H^+$ and $H^-$ impact on H and $H_2$, Phys. Rev. A, 36, 3091-3099, 1987.

Iyemori, T., and D. R. K. Rao, Decay of the Dst component of geomagnetic disturbance after substorm onset and its implication to storm substorm relation, Ann. Geophys., 14, 608-618, 1996.

Milan, S. E., M. Lester, S. W. H. Cowley, and M. Brittnacher, Dayside convection and auroral morphology during an interval of northward interplanetary magnetic field, Ann. Geophysicae, 18, 436-444, 2000.

Meng, C.-I., Case studies of the storm time variations of the Polar cusp, J. Geophys. Res., 88, 137-149, 1983.

Moore, T. E., et al., The thermal ion dynamics experiment and plasma source instrument, Space Sci. Rev., 71, 409, 1995.

Moore, T. E., et al., The low-energy neutral atom imager for IMAGE, Space Sci. Rev., 91(1-2), 155-195, 2000.

Moore, T. E. et al., Low energy neutral atoms in the magnetosphere, Geophys. Res. Lett, 28, 1143-1146, 2001.

Moore, T. E., M. R. Collier, M.-C. Fok, S. A. Fuselier, H. Khan, W.Lennartsson, D. G. Simpson, G. R. Wilson, M. O. Chandler, Heliosphere-Geosphere Interactions Using Low Energy Neutral Atom Imaging, Space Sci. Rev., 109, 351-371, 2003.

Newell, P. T., and C.-I. Meng, The cusp and cleft/boundary: Low altitude identification and statistical local time variations, J. Geophys. Res., 93, 14,549-14,556, 1988.

Newell, P. T., C.-I. Meng, D. G. Sibeck, and R. P. Lepping, Some low-altitude cusp dependencies on interplanetary magnetic field, J. Geophys. Res., 94, 8921-8927, 1989.

Ostgaard, N., S. B. Mende, H. U. Frey, G. R. Gladstone, and H. Lauche, Neutral hydrogen density profiles derived from geocoronal imaging, J. Geophys. Res., 108(A7), 10.1029/2002JA009749, 2003.

Paschmann, G., G. Haerendel, N. Sckopke, and H. Rosenbauer, Plasma and magnetic field characteristics of the distant polar cusp near local noon: The entry layer, J. Geophys. Res., 81, 2883-2899, 1976.

Rairden, R. L., L. A. Frank, and J. D. Craven, Geocoronal imaging with Dynamics Explorer, J. Geophys. Res., 91, 13,613-13,630, 1986.

Roelof, E. C., and A. J. Skinner, Extraction of ion distributions from magnetospheric ENA and EUV images, Space Sci. Rev., 91, 437-459, 2000.

Russell, C. T., R. C. Snare, J. D. Means, D. Pierce, D. Dearborn, M. Larson, G. Barr, and G. Le, The GGS POLAR magnetic fields investigation, Space Sci. Rev., 71, 563-582, 1995.

Sandholt, P. E., C. J. Farrugia, L. F. Burlage, J. A. Holtet, J. Moen, B. Lybekk, B. Jacobsen, D. Opsvik, A. Egeland, R. Lepping, A. J. Lazarus, T. Hansen, A. Brekke, and E. Friis-Christensen, Cusp/cleft auroral activity in relation to solar wind dynamic pressure, interplanetary magnetic field $B_z$ and $B_y$, J. Geophys. Res., 99, 17,323-17,342, 1994.

Sandholt, P. E., C. J. Farrugia, M. Oieroset, O. Stauning, and W. F. Denig, Auroral activity associated with unsteady magnetospheric erosion: Observations on December 18, 1990, J. Geophys. Res., 103, 2309-2317, 1998.

Shue, J.-H., et al., Magnetopause location under extreme solar wind conditions, J. Geophys. Res., 103, 17,691-17,700, 1998.

Taguchi, S., M. Sugiura, J. D. Winningham, and J. A. Slavin, Characterization of the IMF By-dependent field-aligned currents in the cleft region based on DE 2 observations, J. Geophys. Res., 98, 1393-1407, 1993.

Taguchi, S., M. R. Collier, T. E. Moore, M.-C. Fok, and H. J. Singer, Response of neutral atom emissions in the low- and high-latitude magnetosheath direction to the magnetopause motion under extreme solar wind conditions, J. Geophys. Res., 109(A4), 10.1029/2003JA010147, 2004.

Takeuchi, T. T. Araki, A. Viljanen, J. Watermann, Geomagnetic negative sudden impulses: Interplanetary causes and polarization distribution, J. Geophys. Res., 107(A7), 10.1029/2001JA900152, 2002.

Wallace, L., C. A. Barth, J. B. Pearce, K. K. Kelly, D. E. Anderson Jr., and W. G. Fastie, Mariner 5 measurement of the Earth’s Lyman alpha emission, J. Geophys. Res., 75, 3769-3777, 1970.

Zhou, X. W., C. T. Russell, G. Le, S. A. Fuselier, and J. D. Scudder, Solar wind control of the Polar cusp at high altitude, J. Geophys. Res., 105, 245-251, 2000.

**Figure Captions**

**Figure 1.** ACE Solar wind data, and SYM-H for the event in this study. (a) Flux of energetic ions with energies between 47 and 65 keV/e (in unit of counts $s^{-1}$ $cm^{-2}$ $ster^{-1}$ $MeV^{-1}$), (b) GSM *Y* component of the magnetic field, (c) GSM *Z* component, (d) solar wind number density, (e) GSM *X* component of velocity, (f) solar wind dynamic pressure, and (g) H-component of the SYM index.

**Figure 2.** Schematic picture showing why the direction of the cusp indentation can be identified with IMAGE/LENA inside the magnetosphere. A bold curve represents the shape of the magnetopause that has the cusp indentation, and the sheath flow along the magnetopause is shown with the black arrows. The green arrows show the direction of possible neutral atom emission created in the cusp indentation.

**Figure 3.** Position of IMAGE and Polar in (a) GSM *X*-*Z* and (b) *X*-*Y* planes for 0500 -0520 UT April 12, 2001. The squares indicate the location of the spacecraft at 0500 UT, and the short black lines from the squares represent the motion of the spacecraft during 0500-0520 UT. Two arrows from a point on the IMAGE orbit represent a 120˚ (=217˚ minus 97˚) field of view of LENA that is used for our analysis.

**Figure 4.** LENA snapshot obtained around 0508 UT April 12, 2001. Background corrected scaled hydrogen count rates are plotted in the format of the spin angle versus the Polar angle. The cusp indentation signal and the Sun signal can be seen.

**Figure 5.** LENA image mapped on a sphere surface with a radius of 8 $R_E$ for (a) 0505-0507 UT, (b) 0507-0509 UT, and (c) 0509-0511 UT. The hydrogen count rate for each LOS is plotted at the ($Y_{GSM}$, $Z_{GSM}$) position of the intersection on the sphere. The count rate data in (b) are the same as those for Figure 4. The white cross mark in shows the location of the peak emission occurring at higher latitudes, *i.e.*, the cusp indentation signal. The red mark in (c) indicates the peak of the signal at lower-latitudes.

**Figure 6.** Comparison between the Polar (Panels a-f), IMAGE/LENA (Panel g), and ACE (Panel h) observations during the period 0500-0520 UT. Magnetic field data obtained by Polar are shown in the top four panels (Panels a, b, c, and d). Panels e and f are the spectrogram in the spin angle versus UT, and the one in the format of energy versus UT, respectively. In Panel e, the – (+) sign indicates the direction (opposite direction) of the magnetic field projected on the spin plane with respect to the spacecraft moving direction indicated by × sign. They also indicate parallel (anti-parallel) flows along + (–) direction. Panel g shows the LENA normalized counts in each time and range bin. The red color indicates the spin angle for the maximum count in each time. The vertical two lines represent the interval of the cusp observations, which is determined with the magnetic field depression and the higher energy flux of the ions. Panel h shows the IMF $B_Z$ variations observed by ACE.

**Figure 7.** Schematic illustration of the interpretation of the simultaneous observations from IMAGE/LENA and Polar/TIDE around 0510 UT on April 12, 2001. The solid arrow in the shaded region represents the flow of the ion entry, and the curved arrows in the indentation show the sheath plasma flow. The dashed green lines from the arrows

represent the emission of the neutral atoms. The longest green line from the black arrow represents the emission that reaches the position of IMAGE.

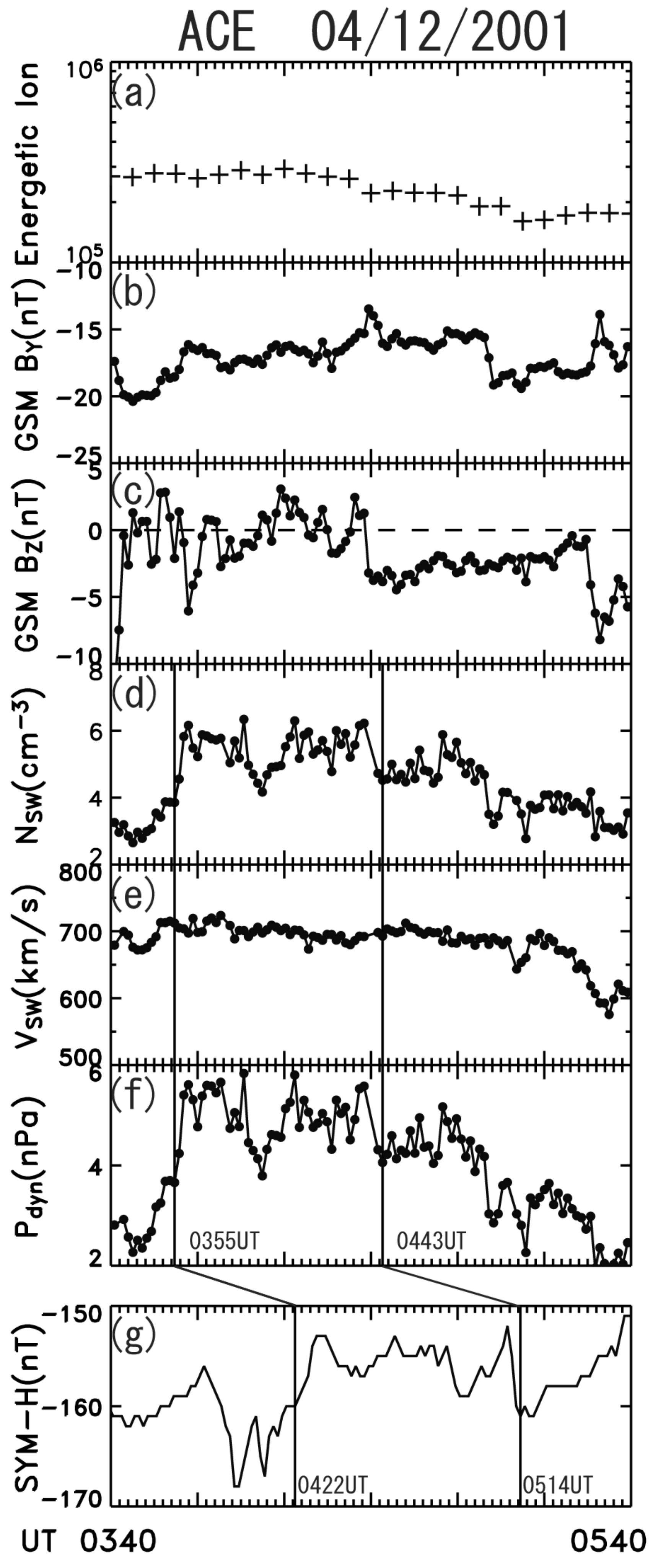
ACE 04/12/2001
Energetic Ion
GSM $B_Y$(nT)
GSM $B_Z$(nT)
$N_{SW}$(cm$^{-3}$)
$V_{SW}$(km/s)
$P_{dyn}$(nPa)
SYM-H(nT)
0355UT
0443UT
0422UT
0514UT
UT 0340
0540

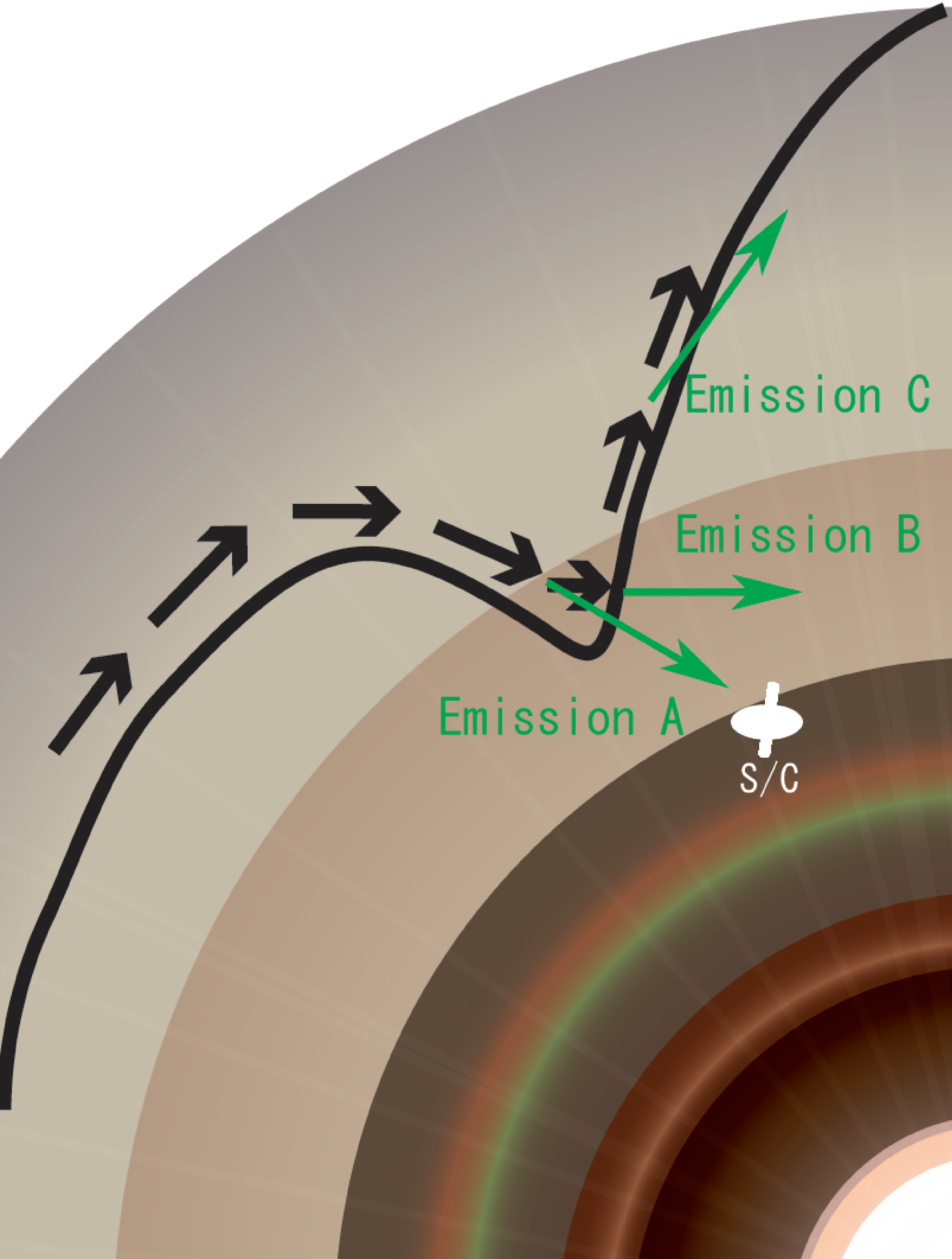
Emission C
Emission B
Emission A
S/C

04/12/2001 0500-0520 UT
(a)
Spin Angle 217°
IMAGE
Spin Angle 97°
POLAR
Z_GSM (R_E)
X_GSM (R_E)
(b)
IMAGE
POLAR
Y_GSM (R_E)
X_GSM (R_E)

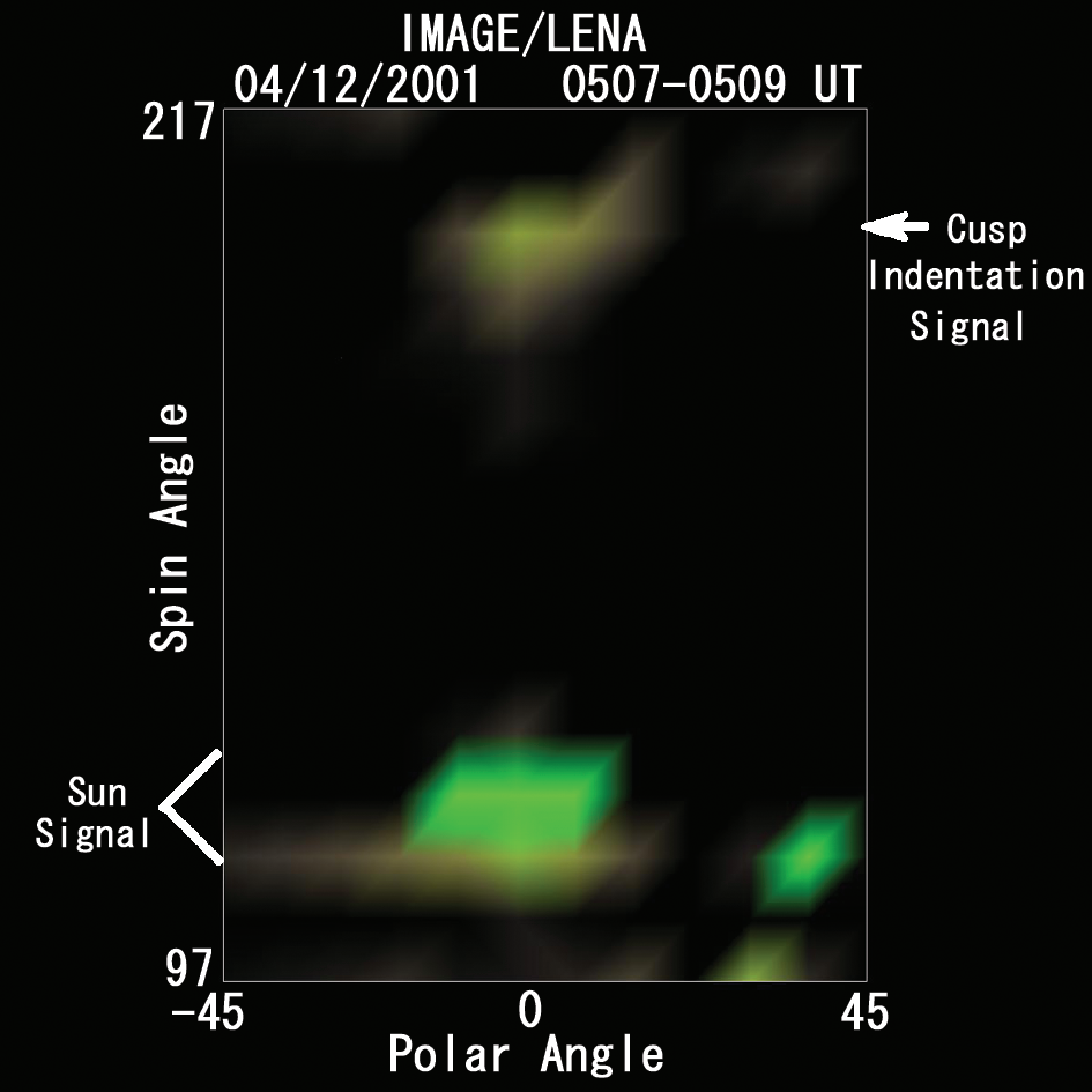
IMAGE/LENA
04/12/2001 0507-0509 UT
217
97
Spin Angle
-45
0
45
Polar Angle
Cusp
Indentation
Signal
Sun
Signal

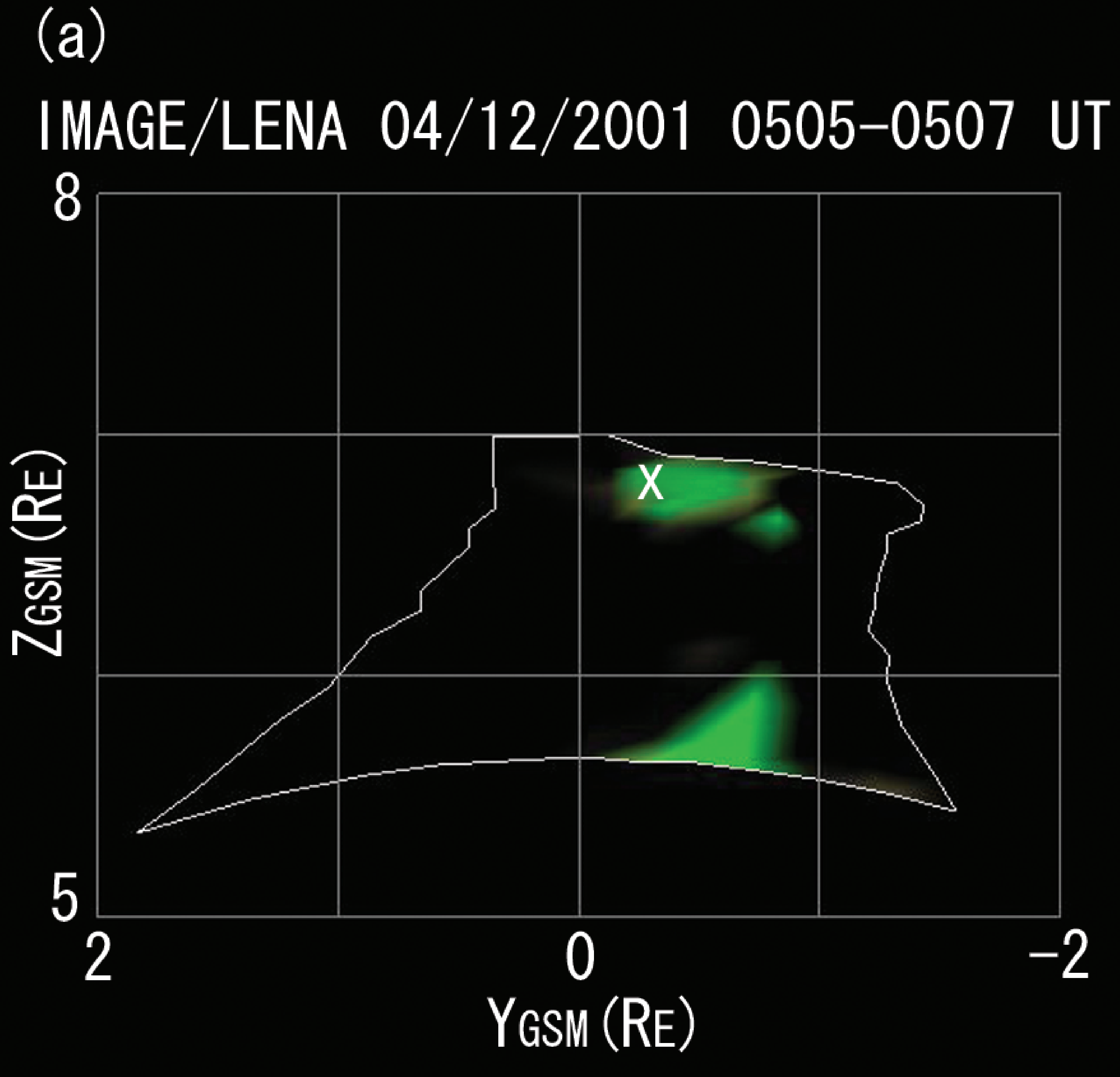
(a)
IMAGE/LENA 04/12/2001 0505-0507 UT
8
5
2
0
−2
X
ZGSM (RE)
YGSM (RE)

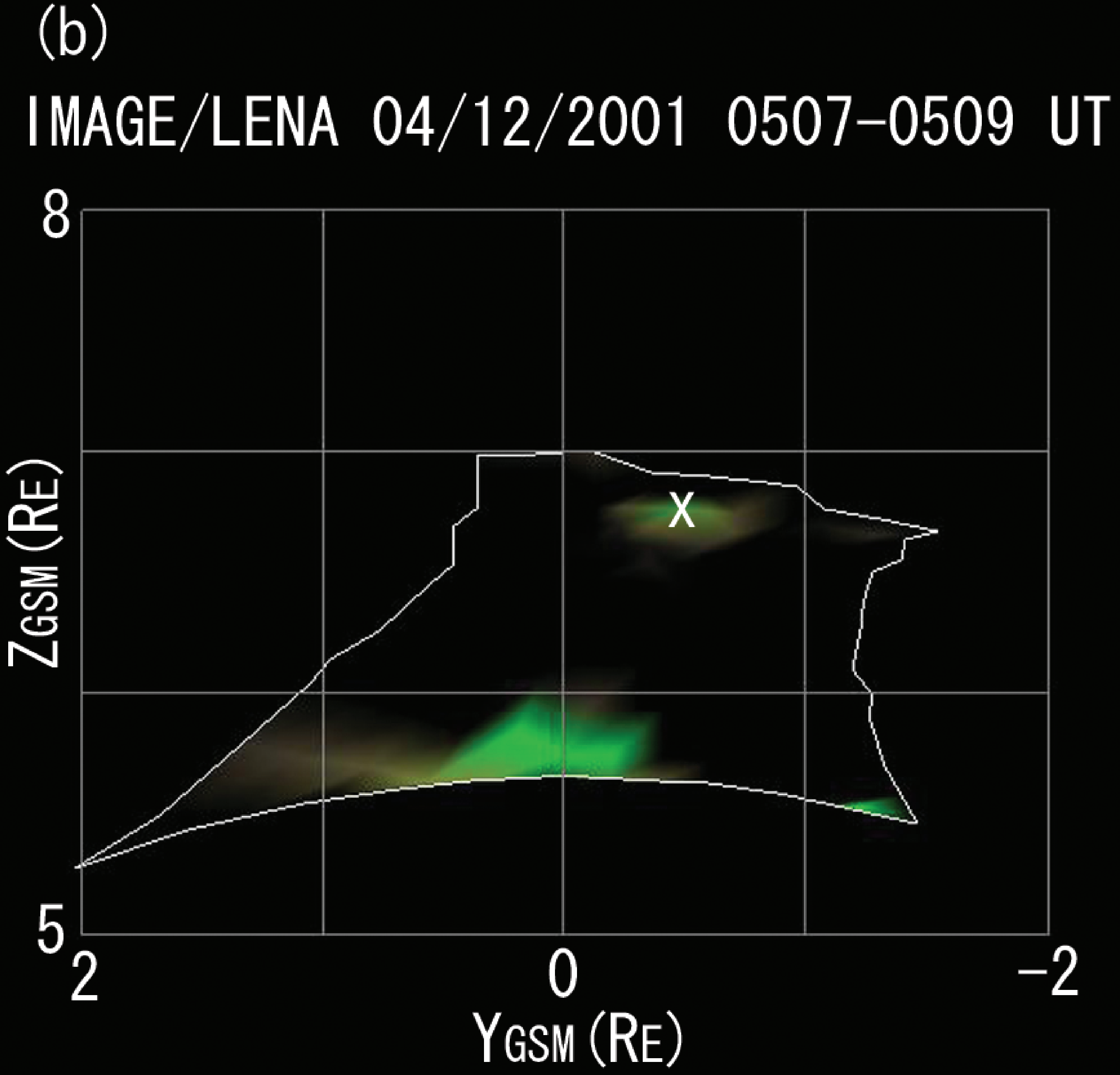

(b)
IMAGE/LENA 04/12/2001 0507-0509 UT
8
5
X
ZGSM (RE)
2
0
−2
YGSM (RE)

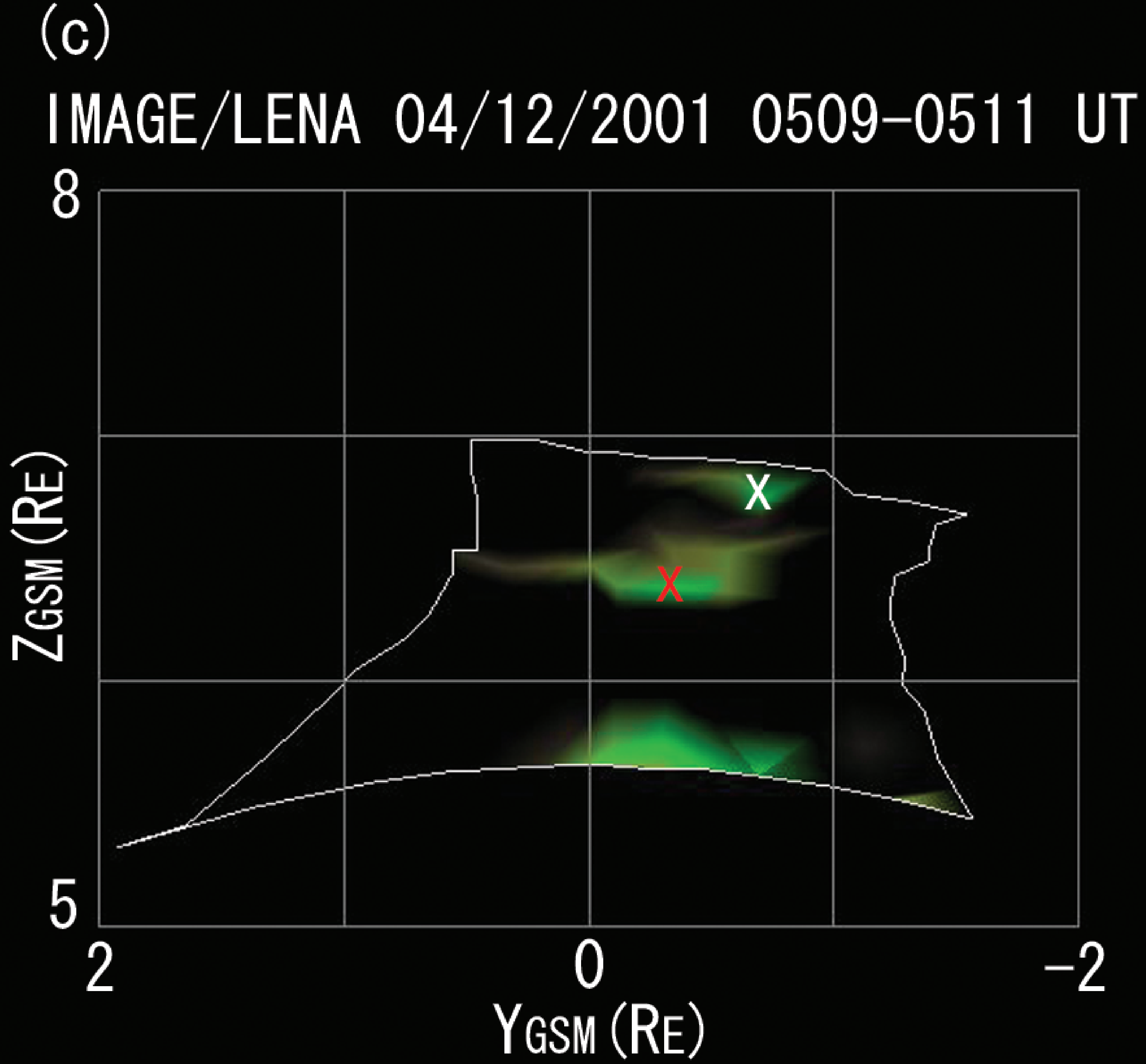
(c)
IMAGE/LENA 04/12/2001 0509-0511 UT
8
5
$Z_{GSM}$ (RE)
2
0
−2
$Y_{GSM}$ (RE)
X
X

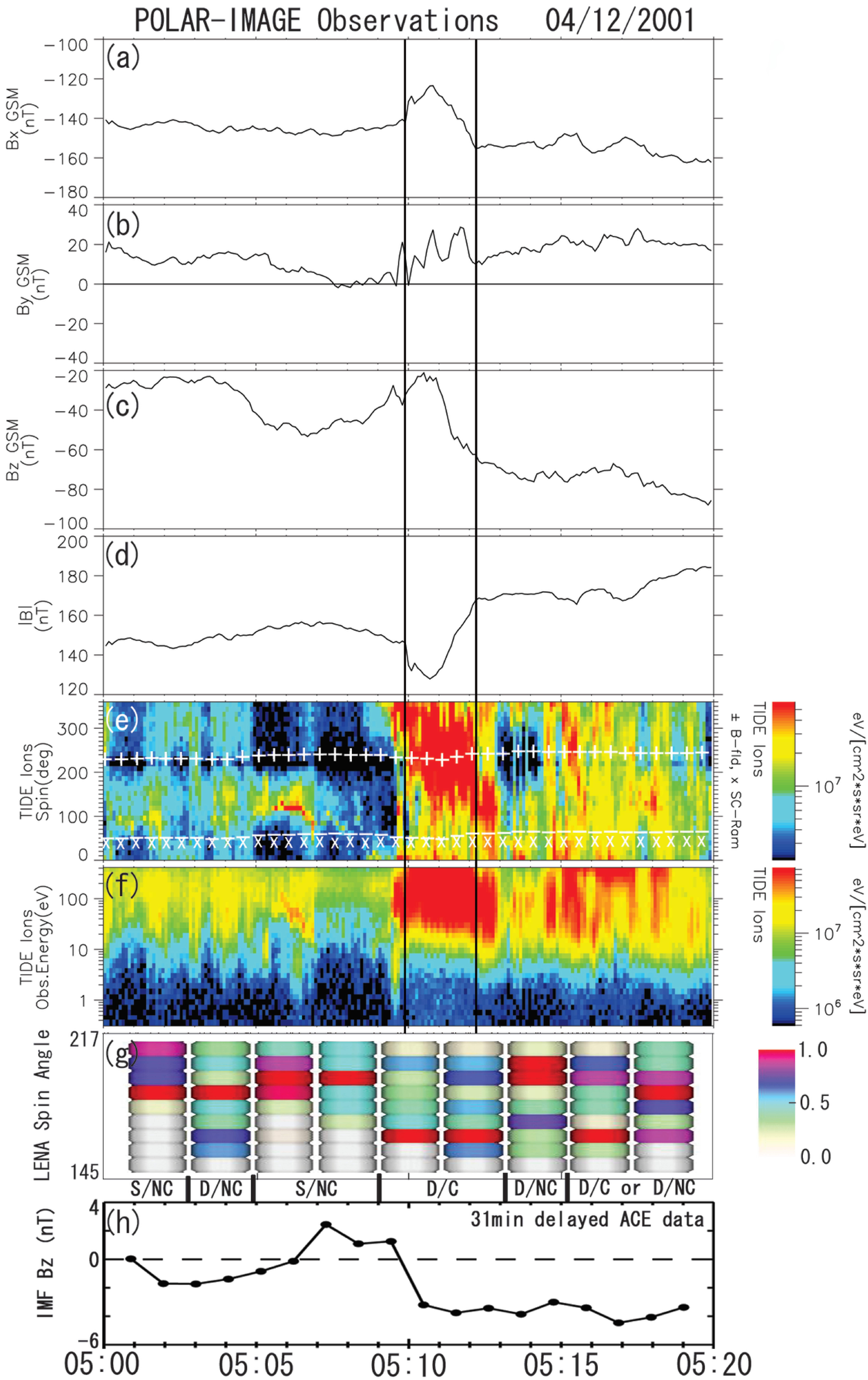
POLAR-IMAGE Observations 04/12/2001
(a)
Bx GSM (nT)
(b)
By GSM (nT)
(c)
Bz GSM (nT)
(d)
|B| (nT)
(e)
TIDE Ions Spin(deg)
± B-fld, x SC-Ram
TIDE Ions
eV/[cm^2*s*sr*eV]
(f)
TIDE Ions Obs.Energy(eV)
TIDE Ions
eV/[cm^2*s*sr*eV]
(g)
LENA Spin Angle
S/NC
D/NC
S/NC
D/C
D/NC
D/C or D/NC
(h)
IMF Bz (nT)
31min delayed ACE data
05:00
05:05
05:10
05:15
05:20

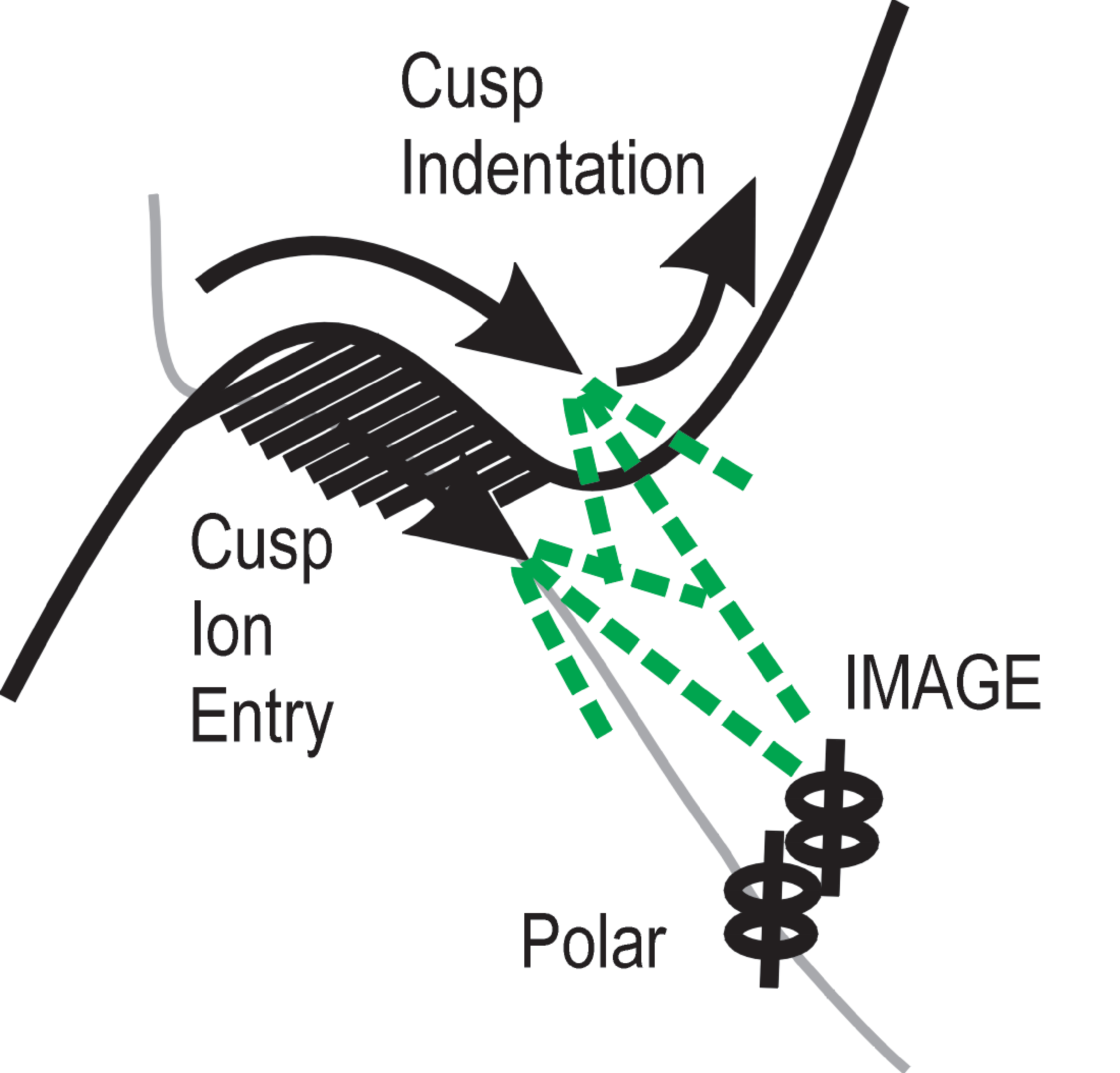
Cusp
Indentation
Cusp
Ion
Entry
IMAGE
Polar